Revista Ingeniería Biomédica
ISSN 1909–9762, volumen 3, número 5, enero-junio 2009, págs. 33-42
Escuela de Ingeniería de Antioquia–Universidad CES, Medellín, Colombia

Image-quality optimization for dual energy computed tomography (DECT) three-material decomposition

Optimización de la calidad de la imagen para la separación de tres materiales utilizando la tomografía computarizada de dos energías (TCDE)

Carolina Arboleda Clavijo[1,Ψ], Norbert J. Pelc, Sc.D[2]
[1] *Biomedical Engineering Program. Escuela de Ingeniería de Antioquia-Universidad CES*
[2] *Professor of Radiology and Bioengineering, Professor of Electrical Engineering by courtesy, Associate Chair for Research, Radiology, Stanford University, CA, United States of America*

Received March 17, 2008. Accepted April 28, 2009.

***Abstract*—** Dual energy computed tomography, which consists of the acquisition of two images of a given region of interest using two different x-ray energies, has been used to decompose images. For example, it has been proposed to estimate the degree of stenosis of blood vessels with calcified plaques. Pragmatic realities, though, such as beam hardening, scattered radiation and mostly quantum noise, reduce the ideal of a perfect decomposition.

In this study, a dual energy separation method for iodinated contrast media, cortical bone and soft tissue was implemented; afterwards, it was tested in simulated noiseless and noisy situations. The noise propagation was modeled mathematically, and an image-quality optimization technique regarding the right distribution of radiation dose between the high and low energy images was proposed. The results obtained suggest that in the absence of noise and using mono-energetic beams, an accurate separation is possible, but when noise is added and poly-chromatic spectra used this decomposition becomes more challenging.

***Keywords*—** Dual energy computed tomography, Image-quality optimization technique, Linear attenuation coefficient, Material-decomposition algorithms, Noise propagation, Radiation dose.

***Resumen*—** La tomografía computarizada de dos energías, que consiste en la adquisición de dos imágenes de una región de interés dada usando rayos X de dos energías distintas, ha sido utilizada para descomponer imágenes. Por ejemplo, esta técnica ha sido propuesta para estimar el grado de estenosis de vasos sanguíneos obstruidos con placas de calcio. Sin embargo, fenómenos como el endurecimiento del rayo, la radiación dispersada y principalmente el ruido cuántico, impiden que esta separación sea perfecta.

En este estudio, se implementó un método de separación de medio de contraste yodado, tejido blando y hueso cortical; este se evaluó en simulaciones, tanto en presencia como en ausencia de ruido. Posteriormente, se modeló matemáticamente la propagación del ruido y, con base en los resultados de estos modelos, se propuso una técnica de optimización de la imagen basada en la distribución adecuada de la dosis de radiación entre las imágenes de energías alta y baja. Los resultados evidencian que en ausencia de ruido y con rayos mono-energéticos, es posible obtener una separación precisa, pero cuando se adiciona ruido a las imágenes y se trabaja con espectros policromáticos, la descomposición resulta más complicada.

***Palabras clave*—** Tomografía computarizada de dos energías, Técnicas de optimización de la calidad de la imagen, Coeficiente de atenuación lineal, Algoritmos de separación de materiales, Propagación del ruido, Dosis de radiación.

I. Introduction

Computed tomography images are produced from a large number of x-ray transmission measurements. The detector measures an x-ray intensity, I_t, that for an uniform object and a mono-energetic beam is related to the unattenuated intensity I_0 according to the following equation, where t is the thickness of the object along the ray and μ is the average linear attenuation coefficient [1-2]:

$$I_t = I_0 e^{-\mu t}$$

For inhomogeneous objects:

$$I_t = I_0 e^{-\int \mu(t)\, dt}$$

where μ(t) is the distribution of linear attenuation coefficients. In computed tomography, a reconstruction algorithm computes the distribution of μ across the objects from the transmission measurements in all directions.

In CT, the use of iodinated contrast agents, which have a high attenuation coefficient, causes the iodine-filled blood vessels to appear much brighter than the surrounding tissue (mainly composed of water). In the case of vessels with a soft tissue plaque, this technique allows for accurate diagnosis of the degree of stenosis. Calcified plaque, however, introduces inaccuracies that limit the use of CT, due to the excessively bright plaque that overshadows the nearby regions, a phenomenon known as blooming. The blooming effect of calcium prevents calculation of the exact size of the patent portion of the lumen [3].

The use of dual energy CT (DECT) has been proposed to solve this problem [4-6]. This technique consists of the acquisition of two images of a given region of interest using two different x-ray wavelengths. A weighted subtraction of these two images would ideally result in an image in which calcium has the same intensity as the surrounding tissue while the iodine-filled lumen remains bright [7].

Different researchers have proved the promises of DECT to separate iodine and bone filled vessels. In 2005, T.G. Flohr and others scanned a piece of pork containing bone, metal pieces, and tubes filled with solutions of iodine with different densities; this specimen was inserted in a tank of water. They used a SOMATON Dual-source CT system (Siemens Medical Solutions), where Tube A was set to 80 keV and 350 mA and Tube B to 140 keV and 150 mA, and obtained a successful bone-iodine separation [8]. More recently, in 2008, X. Liu and other researchers from Mayo Clinic, proposed and validated a mass-conservation based three-material decomposition DECT algorithm, obtaining accurate measurements of the elemental concentrations of the materials under low noise imaging conditions [9].

With the purpose of analyzing the influence of quantum noise on DECT decomposition algorithms and looking for a way to reduce it regarding dose considerations, a dual energy algorithm for the iodine-soft tissue-bone decomposition was implemented in this study. A Poisson-based noise model was used, and the noise propagation was modeled mathematically and compared with the results obtained with simulated data in noiseless and noisy cases, using both mono-energetic and poly-energetic spectra. Based on these results, an optimization technique regarding the noise performance and the optimal distribution of radiation dose between the high and low energy images was proposed. This project focused on reducing the quantum noise and beam hardening effects were neglected. These effects can be considered and analyzed in future studies.

II. Materials and methods

2.1 Phantoms

All the phantoms were defined using CATSIM 2.1 (GE Global Research, Niskayuna, NY). The main phantom corresponds to an axial slice of the human thorax (Fig. 1). It has one healthy blood vessel (100% iodine solution, right top), one vessel with a soft tissue plaque (center top, below the sternum) and a vessel with a calcified plaque (bottom) (Fig. 2), both with a degree of stenosis of 80%, and all the blood vessels with a diameter of 3 mm. Both plaques (soft tissue and cortical bone) have the same size. It was assumed that the soft tissue linear attenuation coefficient was completely equivalent to water's, and that each voxel of the phantom was exclusively made of water, iodinated contrast agent and bone, as follows:

$$1 = f_{Water} + f_{Bone} + f_I$$

Where fWater, fBone, fI correspond, respectively, to the volume fractions of water, bone and iodine.

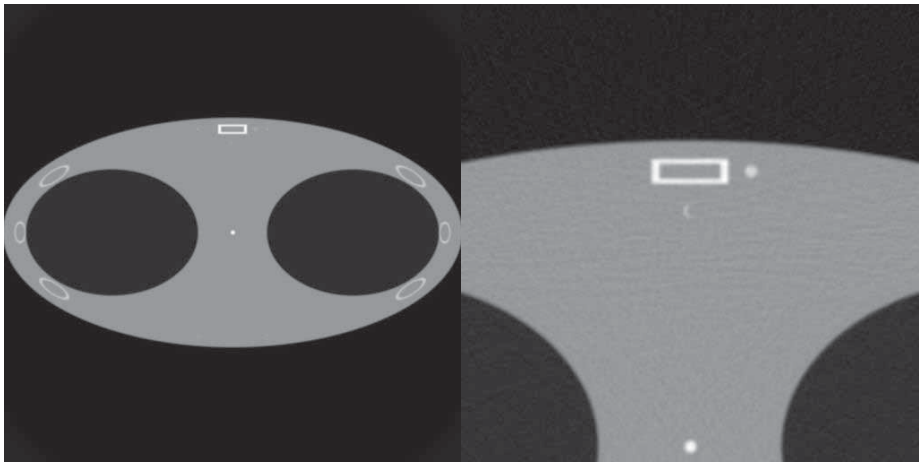

Fig.1. Thorax phantom. Left: full field of view. Right: region of interest at 120 KeV. Calcium blooming can be evidently seen.

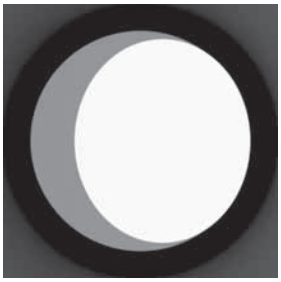

Fig.2. A blood vessel with a calcified plaque and a degree of stenosis of 80%, at 120 keV.

To assure that the attenuation coefficients would be consistent, a calibration phantom was designed (Fig. 3).

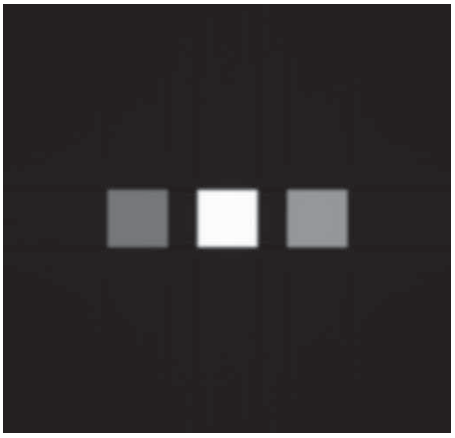

Fig.3. Calibration phantom at 120 keV. From left to right (in the boxes): water, bone and iodine solution 1.2%w/w.

2.2 3-material decomposition algorithm

To find out the fraction f of each material with a respective linear attenuation coefficient μ, the following system of linear equations was solved using algorithms written in MATLAB 7.0:

$$\mu_{low\ energy} = \mu_{11} f_{Water} + \mu_{12} f_{Bone} + \mu_{13} f_I \quad (1)$$

$$\mu_{high\ energy} = \mu_{21} f_{Water} + \mu_{22} f_{Bone} + \mu_{23} f_I \quad (2)$$

$$1 = f_{Water} + f_{Bone} + f_I \quad (3)$$

Where:

μ_{11}: water linear attenuation coefficient (LAC) at low energy.

μ_{12}: bone LAC at low energy.

μ_{13}: iodine LAC at low energy.

μ_{21}: water LAC at high energy.

μ_{22}: bone LAC at high energy.

μ_{23}: iodine LAC at high energy.

f_{Water}, f_{Bone} and f_I correspond to the volume fractions of water, bone and Iodine, in that order; and $\mu_{lowenergy}$ and $\mu_{highenergy}$ to the LAC of each voxel at the low and high energies, respectively. This system is based on the dual energy basis material decomposition [10].

Several phantoms were reconstructed, using different w/w (weight/weight) concentrations of iodine for the iodinated solution (1.2%, 2.4% and 5% w/w of I dissolved in water, respectively). The idea was to analyze the performance of the algorithm of separation with respect to these concentrations, although current injection protocols commonly achieve the lowest one [11].

The system presented above can be written as follows:

$$\underbrace{\begin{bmatrix} \mu_{11} & \mu_{12} & \mu_{13} \\ \mu_{21} & \mu_{22} & \mu_{23} \\ 1 & 1 & 1 \end{bmatrix}}_{A} \underbrace{\begin{bmatrix} f_{Water} \\ f_{Bone} \\ f_I \end{bmatrix}}_{x} = \underbrace{\begin{bmatrix} \mu_{lowenergy} \\ \mu_{highenergy} \\ 1 \end{bmatrix}}_{b}$$

Hence, three images are obtained: f_{Water}, f_{Bone} and f_I.

2.3. Calculation of the noise propagation

Since $x=A^{-1}b$, the error propagation can be calculated as:

$$\sigma^2{}_x = \left(\frac{\partial x}{\partial \mu_{lowenergy}}\right)^2 \sigma^2{}_{lowenergy} + \left(\frac{\partial x}{\partial \mu_{highenergy}}\right)^2 \sigma^2{}_{highenergy} \quad (4)$$

Assuming that the high energy attenuation coefficient measurements are totally independent from the low energy ones (the covariance was assumed to be zero). X corresponds either to the water fraction, bone fraction or the iodine fraction images.

To calculate $\sigma^2_{lowenergy}$ and $\sigma^2_{highenergy}$, a region of water of 180x180 (32400) pixels located in the center of the region of interest, was selected.

2.4 Optimization technique to reduce the noise

2.4.1 Mono-energetic beams

Although real CT-scanners work with polychromatic beams, it is interesting for the purposes of this study to analyze what happens when mono-energetic beams are used [12]. The software CATSIM 2.1 was used to simulate this case.

X-ray and γ-ray counting statistics obey the Poisson distribution. Hence, knowing the mean implies that σ (called the standard deviation or the noise) is known. Therefore, the noise in an image can be adjusted by adjusting the (mean) number of photons used to produce the image [1].

Noise as perceived by the human observer in an image is the relative noise, also called the coefficient of variation (COV) [13]:

$$\sigma_x = COV = \frac{1}{\sqrt{N}}$$

Thus, as N is increased in an image, the relative noise decreases and the SNR (Signal-to-noise ratio), which is the inverse of the COV, increases by the same factor √N [1].

In a transmission measurement, the key determinant is the number of x-ray photons detected [12]. Therefore, we define the relative noise as:

$$\sigma_x = \frac{1}{\sqrt{N_{detected}}} \; or \quad \sigma^2_x = \frac{1}{N_{detected}} \qquad (5)$$

For transmission through an object of thickness t and attenuation coefficient μ [1]:

$$N_{detected} = N_0 e^{-\mu t} \quad (6),$$

Where N_0 is the number of incident photons.

Radiation dose is proportional to the energy fluence. For a dual energy scan, the total energy fluence can be approximated as follows:

$$D = N_{01} E_1 + N_{02} E_2 \qquad (7)$$

N_{0i} represents the number of incident photons/(s)(cm^2) (A) used to obtain the i^{th} image ($i=1$ is low energy, $i=2$ is high energy) and Ei the energy (in keV) that is being used for each case respectively. As we can see, an infinite number of choices of E_1, E_2, N_{01} and N_{02}, deposits the same energy fluence (and hence the same dose). However, they will have different noise behavior. We seek the ideal allocation of energy fluence.

(7) Can be rewritten as:

$$1 = \frac{N_{01} E_1}{D} + \frac{N_{02} E_2}{D} \quad (8)$$

We define $f_1 = \frac{N_{01} E_1}{D}$ as the fraction of the total energy fluence allocated to the low energy image, then:

$$N_{01} = \frac{f D_1}{E_1} \quad (9) \text{ and}$$

$$N_{02} = \frac{D(1-f_1)}{E_2} \quad (10)$$

To calculate the number of detected photons in both the low and high energy image (N_1 and N_2, respectively) , we can replace (9) and (10) in (6) as follows:

$$N_1 = \frac{f D_1}{E_1} e^{-\mu_1 t} \quad (11) \text{ and}$$

$$N_2 = \frac{D(1-f_1)}{E_2} e^{-\mu_2 t} \quad (12)$$

The partial derivatives presented in (4) are constant and just depend on the attenuation coefficients of the materials that are being separated [14]. Therefore, and considering (5), (11) and (12), the noise generated in each individual material image is independent and thus can be written as:

$$\sigma^2_x = c_1 \frac{e^{\mu_1 t} E_1}{f D_1} + c_2 \frac{e^{\mu_2 t} E_2}{D(1-f_1)} \quad (13)$$

Where

$$c_1 = \left(\frac{\partial x}{\partial \mu_{lowenergy}}\right)^2 \; and \; c_2 = \left(\frac{\partial x}{\partial \mu_{highenergy}}\right)^2$$

To optimize the signal to noise ratio (SNR), and hence the quality of the image, σ^2_x should be as low as possible. Consequently, the idea is to find out a value for f_1 that minimizes (13). Let:

$$\frac{\partial \sigma^2{}_x}{\partial f_1} = 0$$

After solving the partial derivative, we obtain:

$$f_1 = \frac{-c_1 E_1 e^{\mu_1 t} + \sqrt{c_1 E_1 c_2 E_2 e^{(\mu_2+\mu_1)t}}}{c_2 E_2 e^{\mu_2 t} - c_1 E_1 e^{\mu_1 t}} \quad (14)$$

This was done based on the iodine image noise (X=iodine). Thus, c_1 and c_2 are defined as follows:

$$c_1 = \left[\frac{\mu_{22} - \mu_{21}}{(\mu_{22} - \mu_{21})(\mu_{13} - \mu_{11}) - (\mu_{12} - \mu_{11})(\mu_{23} - \mu_{21})} \right]^2 \quad (15)$$

$$c_2 = \left[\frac{\mu_{12} - \mu_{11}}{(\mu_{22} - \mu_{21})(\mu_{13} - \mu_{11}) - (\mu_{12} - \mu_{11})(\mu_{23} - \mu_{21})} \right]^2 \quad (16)$$

2.4.2 Poly-energetic beams

Real clinical CT scanners work with polychromatic beams and, thus, it is useful to analyze the noise propagation in this case. To the simplest approximation, these beams can be treated as mono-energetic beams with an effective attenuation coefficient. Therefore, for an energy integrating detector, an effective μ for each material can be calculated as follows [14]:

$$\mu_{effective} = \frac{\sum_E En_E \, exp(-\mu_E t)\mu(E)}{\sum_E En_E \, exp(-\mu_E t)} \quad (17)$$

with n_E being the number of photons/(second)(A)(cm^2) with energy E and t the thickness of the object.

For polychromatic spectra and an energy integrating detector, the noise (for both the low and the high energy images) is further computed as [13]:

$$\sigma = \frac{\sqrt{\sum_E E^2 N_E \exp(-\mu_E t)}}{\sum_E E N_E \exp(-\mu_E t)} \quad (18)$$

with N_E being the number of photons with energy E.

If we assume a current-time product (mA*s) C_1 for the low energy beam, a (mA*s) C_2 for the high energy one, and an individual detector area of 1 mm^2, (18) can be re-written as follows for the low and high energy images, respectively:

$$\sigma_l = \underbrace{\frac{\sqrt{\sum_E E^2 (n_E \text{ x } 10^{-5})\, C_1 \, exp(-\mu_E t)}}{\sum_E E\,(n_E \text{ x } 10^{-5}) C_1 \, exp(-\mu_E t)}}_{r_1} \quad (19)$$

$$\sigma_H = \underbrace{\frac{\sqrt{\sum_E E^2 (n_E \text{ x } 10^{-5})\, C_2 \, exp(-\mu_E t)}}{\sum_E E\,(n_E \text{ x } 10^{-5}) C_2 \, exp(-\mu_E t)}}_{r_2} \quad (20)$$

Thus, the noise we obtain in the iodine image can be written as:

$$\sigma^2{}_x = \frac{c_1}{C_1 \times 10^{-5}} \times \frac{\sum_{LE} E^2 n_E \exp(-\mu_E t)}{\left[\sum_{LE} E\, n_E \exp(-\mu_E t)\right]^2} + \frac{c_2}{C_2 \times 10^{-5}} \times \frac{\sum_{HE} E^2 n_E \exp(-\mu_E t)}{\left[\sum_{HE} E\, n_E \exp(-\mu_E t)\right]^2} \quad (21)$$

If we consider the same constant energy fluence as above, we can express it as:

$$\underbrace{I \sum_{120} En_E}_{D_p} = C_1 \underbrace{\sum_{LE} En_E}_{j1} + C_2 \underbrace{\sum_{HE} En_E}_{j2} \quad (22)$$

$$D_p = C_1 j_1 + C_2 j_2$$

$$C_2 = \frac{D_p - C_1 j_1}{j_2} \quad (23)$$

Then, we replace (23) in (21) and, as in the mono-energetic case, we let $\frac{\partial \sigma^2{}_x}{\partial C_1} = 0$, to find a value for C_1 that minimizes the noise. Thus:

$$C_1 = \frac{-D_p c_1 j_1 r_1 + \sqrt{(D_p c_1 j_1 r_1)^2 + (c_2 j_1 r_2 j_2 - c_1 j_1^{\,2} r_1)(c_1 D_p^{\,2} r_1)}}{(c_2 j_1 r_2 j_2 - c_1 j_1^{\,2} r_1)} \quad (24)$$

2.5 Experiments

All the experiments were developed performing simulations in CATSIM 2.1 and Freemat v. 2.0.

Simulation parameters were set to the following values, because they are equivalent to those commonly used by real CT scanners:

Table 1. Simulation parameters.

PARAMETER	VALUE
Source to iso-center distance	541 mm
Detector to iso-center distance	408.075 mm
Number of columns in the detector	888
Number of rows in the detector	1
Column size	1.0239 mm
Row size	1.0915 mm
Number of samples to represent f in x direction	3
Number of samples to represent f in y direction	3
Detector column oversampling	3
Detector row oversampling	3
Number of views per rotation	984

For the reconstruction of the phantom, the 2D fan beam reconstruction algorithm that CATSIM 2.1 provides was used.

First at all, the decomposition algorithm was tested in a noiseless situation, with both mono-energetic and poly-energetic beams. The ranges considered were: 40 keV-120 keV (mono-energetic) and 70 kVp-150 kVp (poly-energetic). The increasements were in steps of 1 keV/1 kVp respectively. These ranges were selected because the second one is the most commonly used by real CT scanners, and the first one is approximately equivalent to this one, if equivalent mono-chromatic energies are calculated [14].

Afterwards, the algorithm was tested with the pair of mono-energetic beams yielding the lowest amount of noise and a right allocation of the dose and with the same pair, but with "wrong" dose distribution. Likewise, it was evaluated with the pair of poly-energetic beams yielding the lowest amount of noise in the same conditions.

III. Results

3.1 Mono-energetic case

Fig. 4 shows the graph resulting from the noise propagation analysis performed in MATLAB 7.0. The mono-energetic pair (within the range tested) yielding the lowest amount of noise in the iodine image was 50 keV / 120 keV. Fig. 5 displays the images obtained after performing the decomposition algorithm with the pair of mono-energetic beams mentioned above and with no noise added. The window was set to [01] for all the images, where white corresponds to 1 and black to 0.

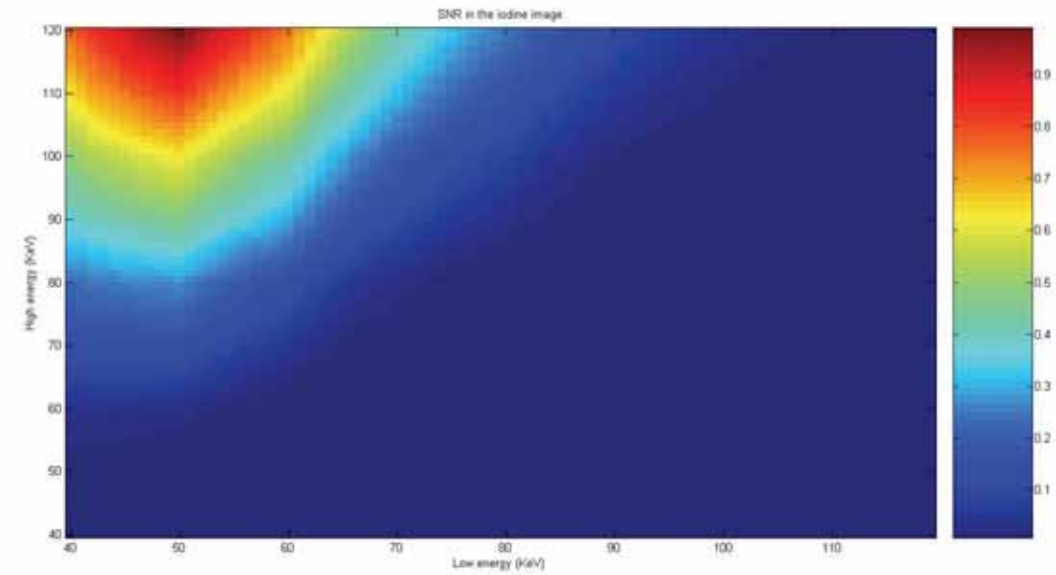

Fig.4. Relative SNR in the iodine image after the decomposition (mono-energetic spectrums). The x-axis corresponds to the low-energy component of the pair of energies used, and the y-axis, to the high energy component.

Fig.5. Fractions of water (left), bone (center) and 1.2% w/w iodine solution (right) after the decomposition, in the noiseless case.

In Fig.5 the ideal dose distribution was used for the pair of mono-energetic beams that yielded the lowest amount of dose in the iodine image (the best result that the dual energy technique can yield in practice). When using a non-optimal dose distribution for the same pair of energies, images presented in Fig. 7 were obtained.

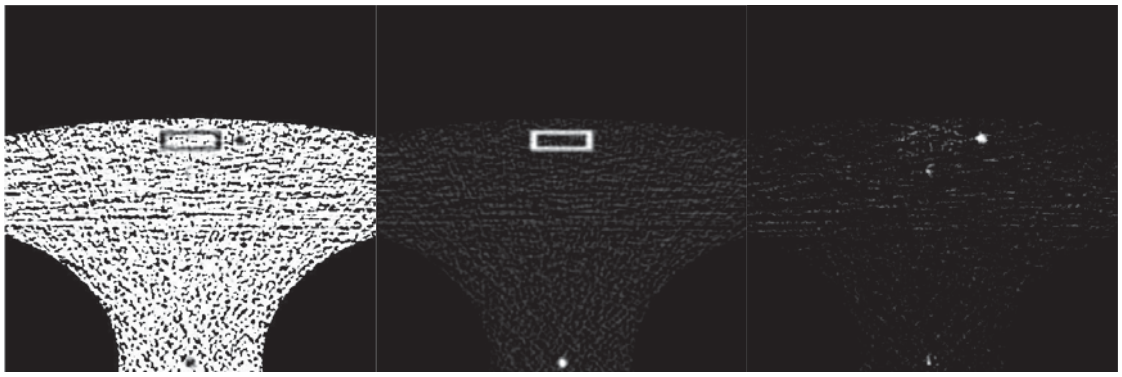

Fig.6. Fractions of water (left, SNR= 1.7416), bone (center, SNR= 0.9367) and iodine solution 1.2% w/w (right, SNR= 0.7561) after the decomposition, noise added, right dose allocation.

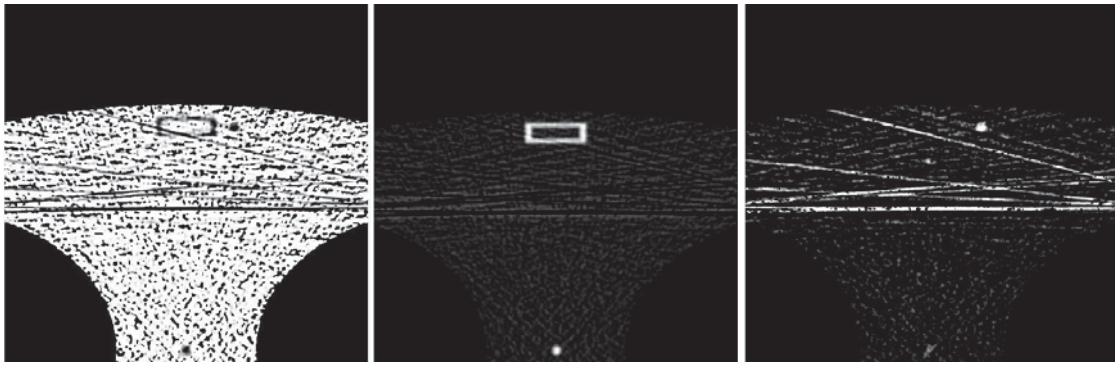

Fig.7. Fractions of water (left, SNR= 1.6381), bone (center, SNR= 0.4458) and iodine solution 1.2% w/w (right, SNR= 0.1824) after the decomposition, noise added, non-optimal dose allocation.

In Fig. 8, the Iodine images obtained after the decomposition, using three different concentrations of Iodine, are shown.

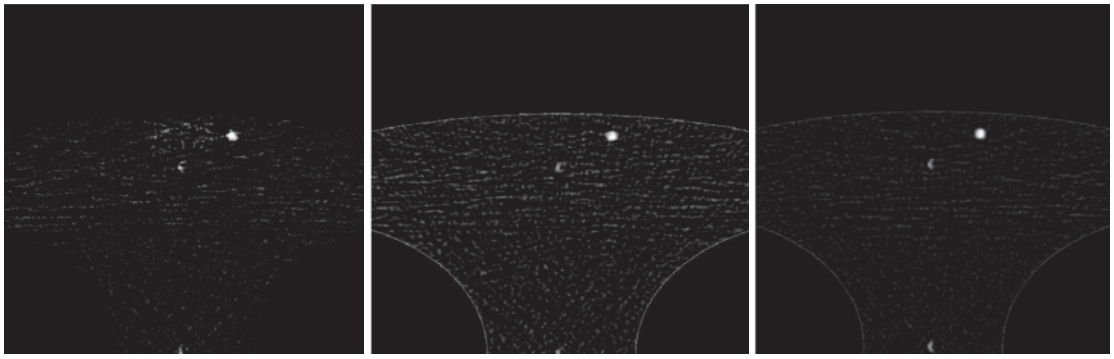

Fig.8. Fractions of iodine solution, 1.2 % w/w (left, σ=0.1309), 2.4 % (center, σ=0.0819) and 5 % (right, σ= 0.0362).

3.2 Poly-energetic case

Fig. 9 shows the graph resulting from the noise propagation analysis performed when using poly-energetic beams. The pair (within the range tested) yielding the lowest amount of noise in the iodine image was 70 kVp / 150 kVp.

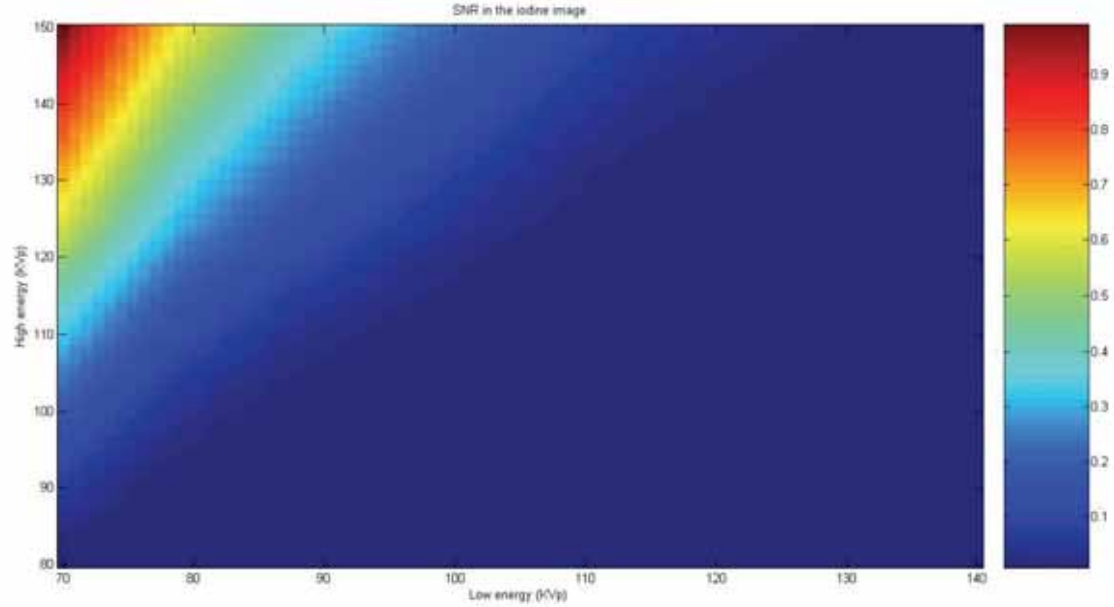

Fig.9. Relative SNR in the iodine image after the decomposition (poly-energetic spectrums, energy-integrating detector).

The results obtained from the decomposition using poly-energetic beams can be seen in Fig. 10 (noiseless), 11 (noisy, correct dose allocation) and 12 (noisy, incorrect dose allocation).

Fig.10. Fractions of water (left), bone (center) and iodine solution 1.2% w/w (right) after the decomposition, in the noiseless case.

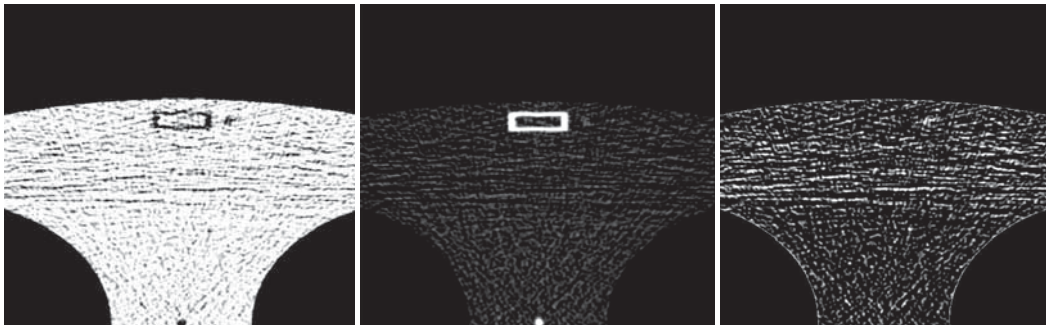

Fig.11. Fractions of water (left, SNR=3.3261), bone (center, SNR= 0.4066) and iodine solution 1.2% w/w (right, SNR=0.2155) after the decomposition, when noise was added, and dose was allocated properly.

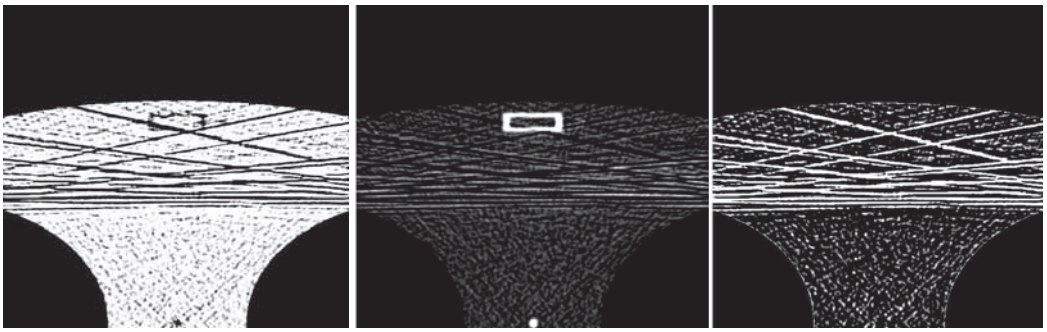

Fig.12. Fractions of water (left, SNR=0.9905), bone (center, SNR=0.1499) and iodine solution 1.2% w/w (right, SNR=0.0384) after the decomposition, when noise added, and dose incorrectly allocated.

IV. Discussion

4.1 Mono-energetic case

As can be seen, when noise is absent, and beams are mono-energetic, the separation algorithm has accurate performance. Here, we are dealing with a well-conditioned linear equation system, and the exactness of the answer depends on the precision of the reconstruction algorithm. The addition of noise impairs the performance of the algorithm, due to the fact that the reconstructed values of μ differ significantly from the ones used for the decomposition matrix. However, as can be seen in Figs. 6 and 7, noise can be appreciably reduced at the same total dose when this one is properly distributed.

Fig. 8 evidences that an increase in the iodine concentration improves notably the performance of the separation algorithm, in spite of the presence of noise. This is due to the fact that as long as there is more iodine in the contrast solution, its attenuation coefficient will differ more from the water's and, therefore, reduce the amount of noise of the individual iodine image. Increasing the concentration of iodine could be considered a way to get better images. However, reaching a higher concentration in vivo may be difficult and safety issues also need to be considered [15].

4.2 Poly-energetic case

An increase in kVp increases the efficiency of x-ray production and the quantity and the quality of the x-ray beam [13] and, therefore, a decrease in the noise. In addition, the noise propagation depends on the behavior of the attenuation coefficients of the materials being separated, at the two energies being considered. Regarding equation (14), it can be inferred that to diminish the noise in the individual iodine image, it is necessary to make c_1 and c_2 as small as possible. As can be deduced from equations (15) and (16), c_1 and c_2 get smaller as the difference between the iodine and water linear attenuation coefficients grows (and so grows the difference between the energies), and thus reduce the propagation of the noise. However, it would be very interesting to evaluate the noise propagation considering a wider range (e.g, 50 kVp-200 kVp); despite it is not achievable in real practice, it would give us more elements to conclude about the noise performance.

The calculation of an effective linear attenuation coefficient implies treating a poly-energetic spectrum as a mono-energetic one [1]. Thus, it disregards the beam hardening effects; this is a possible explanation for the imprecision seen in the decomposition, even in the noiseless case.

The separation algorithm proposed here assumes conservation of the volume. Thus, for mixtures where

this condition can not be achieved, modifications to this algorithm must be implemented, such as those suggested by X. Liu et al [9]. Furthermore, as these researchers concluded, many factors, which were disregarded in this study, such as beam hardening, scattered radiation and partial volume effects affect CT number accuracy and, therefore, the precision of the decomposition [9]. That is why it would be desirable to prove the algorithms presented in this paper using real data, in order to propose effective ways to adequately tackle those factors and analyze their real clinical utility.

V. Conclusion

A dual energy separation method for iodinated contrast media, cortical bone and water was implemented. In a noiseless situation, using mono-energetic spectrums, it was possible to obtain an accurate separation. When using poly-energetic beams without noise, the separation results were affected by beam hardening effects, because in this case the poly-energetic spectra were treated as mono-energetic with an effective linear attenuation coefficient. In order to eliminate the beam hardening artifacts, it would be better to perform the decomposition before the reconstruction. This means working in the projections space instead of the image space.

The outcomes of this algorithm were also analyzed in the presence of noise, using both mono-energetic and poly-energetic spectra. These analyses revealed that the noise propagation is dependent on the pair of energies selected, due to the energy-dependence of the linear attenuation coefficients. Therefore, it is possible to choose a pair of energies that minimizes the noise amplification. Moreover, it was shown that a proper distribution of the radiation dose between the high and low energy images further reduces the noise and improves the remaining lumen visualization.

Increasing the concentration of iodine in the contrast media significantly improves the visualization of the remaining lumen. However, at this point it is necessary to consider the potential adverse reactions that this boost could cause in patients [14].

In conclusion, the results obtained show that dual energy CT could still be considered to separate three materials, if mathematical optimization methods are either performed after or before the reconstruction. The strong energy-dependence of the linear attenuation coefficients continues to be the main motivation for further research in dual energy CT.

Acknowledgement

Thanks to Sam Mazin, Adam Wang and the Richard M. Lucas Center for Medical Imaging, Stanford University, CA, USA.

References

[1] Bushberg J.T., Seibert J.A., Leidholdt E.M., Boone J.M. The essential physics of medical imaging. Lippincot Williams & Wilkins, Second Edition, 2002. P. 330, 323, 277, 278, 279,51, 371-372.

[2] Ramírez J.C., Arboleda C., McCollough C.H. Tomografía computarizada por rayos X: fundamentos y actualidad, Revista Ingeniería Biomédica, 2(4), 54-72, 2008.

[3] Fleischmann D., Hallett R.L., Rubin G.D. CT angiography of peripheral arterial disease. Journal of vascular and interventional radiology: JVIR, 17(1), 3-26, January 2006.

[4] Boll D.T., Hoffmann M.H., Huber N., Bossert A.S., Aschoff A.J., Fleiter T.R. Spectral coronary multidetector computed tomography angiography: dual benefit by facilitating plaque characterization and enhancing lumen depiction. Journal of computer assisted tomography, 30(5), 804-811, 2006.

[5] Johnson T.R., Krauss B., Sedlmair M., Grasruck M., Bruder H., Morhard D., Kink C., Weckbach S., Lenhard M., Schmidt B., Flohr T., Reiser M.F., Becker C.R. Material differentiation by dual energy CT: initial experience. European Radiology, 17(6), 1510-1517, 2007.

[6] Langheinrich A.C., Bohle R.M., Greschus S., Hackstein N., Walker G., Gerlach S., Rau W.S., Hölschermann H. Atherosclerotic lesions at micro CT: feasibility for analysis of coronary artery wall in autopsy specimens. Radiology, 231, 675-681, 2004.

[7] Lehmann L.A., Alvarez R.E., Macovski A., Brody W.R., Pelc N.J., Rieder S.J., Hall A.L. Generalized image combinations in dual KVP digital radiography. Medical physics, 8(5), 659-667, 1981.

[8] Flohr T.G., McCollough C.H., Bruder H., Petersilka M., Gruber K., Süß C., Grasruck M., Stierstorfer K., Krauss B., Raupach R., Primak A.N., Küttner A., Achenbach S., Becker C., Kopp A., Ohnesorge B.M. First performance evaluation of a dual-source CT system. European Radiology, 16(6), 256-258, June 2006.

[9] Liu X., Yu L., Primak A.N., McCollough C.H. Quantitative imaging of element composition and mass fraction using dual energy CT: Three-material decomposition. Medical physics, 36(5), 1602-1609, May 2009.

[10] Álvarez R.E., Macovski A. Energy-selective reconstructions in X-ray computerized tomography. Physics in medicine and biology, 21(5), 733-744, 1976.

[11] Tanikake M., Shimizu T., Narabayashi I., Matsuki M., Masuda K., Yamamoto K., Uesugi Y., Yoshikawa S. Three-dimensional CT angiography of the hepatic artery: use of multi–detector row helical CT and a contrast agent. Radiology. 227(3): 883-889, 2003.

[12] Dilmanian F.A., Wu X.Y., Kress J., Ren B., Chapman D., Coderre J.A., Greenberg D., Parsons E., Shleifer M., Slatkin D.N., Thomlinson W.C., Zhong Z., Button T.M., Giron F., Liang J., Petersen M.J., Roque C.T., Miller M.H., Weedon H., Krus D.J., Perna L., Yamamoto K. Dual energy iodine contrast CT with monochromatic X-rays. Nuclear Science Symposium and Medical Imaging Conference Record, IEEE, 3, 1392-1396, Oct 1995.

[13] Bevington P., Robinson DK., Bevington P., Robinson D.K. Data reduction and error analysis for the physical sciences. Second edition, McGraw-Hill, 41-43, 1992.

[14] Kelcz F., Joseph P.M., Hilal S.K. Noise considerations in dual energy CT scanning. Medical Physics, 6(5), 418-425, September 1979.

[15] Webb J.A.W., Stacul F., Thomsen H.S. Late adverse reactions to intravascular iodinated contrast media. European radiology, 13(1), 181-184, 2003.